THE JOURNAL OF PHYSICAL CHEMISTRY C

Article

Cite This: J. Phys. Chem. C XXXX, XXX, XXX−XXX

pubs.acs.org/JPCC

Long-Term Cycle Behavior of Nano-$LiCoO_2$ and Its Postmortem Analysis

Maziar Ashuri,[†] Qianran He,[†] Zhepu Shi,[†] Changlong Chen,[‡] Weiliang Yao,[†] James Kaduk,[§] Carlo Segre,[∥] and Leon Shaw*[,†]

[†]Department of Mechanical, Materials and Aerospace Engineering, [‡]Department of Chemical and Biological Engineering, [§]Department of Chemistry, and [∥]Department of Physics, and Center for Synchrotron Radiation Research and Instrumentation, Illinois Institute of Technology, Chicago, Illinois 60616, United States

Supporting Information

ABSTRACT: In this study, the long-term cycle behavior of nano-$LiCoO_2$ cathodes over 500 cycles at high rates is investigated. Furthermore, the postmortem analysis of the cycled nano-$LiCoO_2$ cathodes using a combination of X-ray absorption spectroscopy and X-ray diffraction is also conducted to shed light on the capacity decay mechanisms. It is found that crystalline nano-$LiCoO_2$ after 500 charge/discharge cycles at 10C becomes amorphous, exhibits Co^{2+} species rather than the expected Co^{3+} at the fully lithiated condition, has longer Co−O bond length than that of pristine nano-$LiCoO_2$ and micro-$LiCoO_2$, and exhibits 53% specific capacity loss over 500 cycles at 10C. In addition, slow Li-ion intercalation and deintercalation at the electrode/electrolyte interface are found to be the rate-limiting step for nano-$LiCoO_2$ during discharge and charge, respectively. Thus, to achieve the high-rate capability of $LiCoO_2$, not only $LiCoO_2$ particle sizes should be reduced to nanoscales but also the Li-ion intercalation and deintercalation rates at the electrode/electrolyte interface need to be enhanced. Since the capacity decay induced by the structural damage and the formation of CoO-like phases starts at the surface of nano-$LiCoO_2$, proper surface coatings have the potential to solve the capacity decay problem faced by nano-$LiCoO_2$, enabling it for high-rate applications.

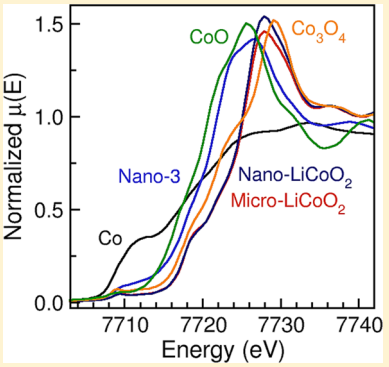

INTRODUCTION

Li-ion batteries have revolutionized portable electronic devices in the past two decades because of their high output voltage, high specific energy, long cycle life, and absence of memory effect.[1] Further improvements in their properties, such as reducing charge time from hours to minutes or extending battery usage time before recharge from 1 day to multiple days, can open up new applications and expand the market for present ones. A case in point for the enormous benefit of short charge time is the continuous effort of electric vehicle manufacturers such as Tesla, Inc. to develop superchargers that can shorten charge time from several hours to about 1 h.[2] A short charge time can enable long-distance travel and remove a significant barrier to consumer acceptance of electric vehicles.[3]

For high specific power and thus short charge time, one needs to address the kinetic problem due to the slow diffusion of Li ions in the electrodes. One approach to increasing the rate capability is to reduce the particle size of the electrode material to nanoscales.[4,5] Nanoparticles can shorten the diffusion distance of Li ions during lithiation/delithiation while increasing the surface area per unit volume for Li-ion intercalation/deintercalation. $LiCoO_2$ being one of the most widely used cathode materials has been investigated for nanosize effects on the rate capability.[4] Through a hydrothermal reaction Okubo et al.[4] have synthesized a series of $LiCoO_2$ nanoplatelets with thickness ranging from 6 to 27 nm and demonstrated the high-rate capability in 20 cycles of charging at 1C and then discharging at 10C. It is shown that the specific capacity drops to about 82 and 30 mA h g^{-1} after 20 cycles for $LiCoO_2$ nanoplatelets of thickness 17 and 8 nm, respectively.[4] Nano-$LiCoO_2$ has also been synthesized through sol−gel method,[6,7] spray-drying method,[8] co-precipitation method,[9] molten salt method,[10,11] and post-templating method.[12] In spite of so many different methods to synthesize nano-$LiCoO_2$, nearly all of the studies[4,6−11] only measure charge/discharge behavior with fewer than 20 cycles, with only one exception that shows charge/discharge behavior over 50 cycles.[12]

In this study, the long-term cycle behavior of nano-$LiCoO_2$ cathodes over 500 cycles is investigated for the first time. In addition, the postmortem analysis of the cycled nano-$LiCoO_2$ cathodes using a combination of X-ray absorption spectroscopy (XAS) and X-ray diffraction (XRD) techniques is also conducted, for the first time, to shed light on the capacity decay mechanisms of nano-$LiCoO_2$ cathodes subjected to fast charge/discharge rates (10C) over 500 charge/discharge cycles. Furthermore, the Li-ion diffusion kinetics with respect

Received: October 16, 2018
Revised: January 16, 2019
Published: January 17, 2019

Downloaded from pubs.acs.org by IOWA STATE UNIV on 01/31/19. For personal use only.
J. Phys. Chem. C

© XXXX American Chemical Society

DOI: 10.1021/acs.jpcc.8b10099
J. Phys. Chem. C XXXX, XXX, XXX−XXX

to $LiCoO_2$ particle sizes and high charge/discharge rates has been analyzed to identify the rate-limiting step in lithiation and delithiation processes. The findings from this study are described below.

METHODS

Nano-$LiCoO_2$ powder was synthesized using the hydrothermal reaction established in ref 4. Briefly, the typical procedure to synthesize a batch of nano-$LiCoO_2$ powder started with the synthesis of CoOOH nanoplates by adding a dilute aqueous solution of 50 mL containing 0.02 mol $Co(NO_3)_2$ into 50 mL of an aqueous 5 M NaOH solution. The resulting $Co(OH)_2$ suspension was then poured into 900 mL of deionized water and stirred in air overnight (~12 h) to produce CoOOH nanoplates. After centrifuging and washing with deionized water twice, the resulting CoOOH was dried in a vacuum oven at 80 °C for 12 h and then 120 °C for 4 h. The dried CoOOH powder of 184 mg was then dispersed in 30 mL of an aqueous 5 M LiOH solution and sealed in a stainless steel autoclave to induce a hydrothermal reaction at 170 °C for 12 h. After the reaction, the resulting precipitate was centrifuged, washed with deionized water twice, and then dried at 100 °C in a vacuum oven for 12 h to give nano-$LiCoO_2$.

Electrochemical testing of the nano-$LiCoO_2$ electrode was performed in CR2032 coin cells through galvanostatic charge/discharge protocols. The electrodes consisted of 75 wt % $LiCoO_2$, 15 wt % carbon black, and 10 wt % poly(vinylidene difluoride) (PVDF). The materials were mixed and hand-ground in a mortar and pestle. *N*-Methyl-2-pyrrolidone was added to form a uniform slurry. The slurry was applied to an Al foil with the loading of ~1.2 mg of $LiCoO_2$ per cm^2. The painted foil was dried in a vacuum oven for 6 h at 60 °C and then 6 h at 120 °C. After drying, the foil was punched to make the working electrode, which was paired with a Li foil serving as both the counter and reference electrode to make CR2032 coin cells. The electrolyte was 1 M lithium hexafluorophosphate ($LiPF_6$) salt dissolved in ethylene carbonate−diethylene carbonate with 1:1 volume ratio. Celgard 2325 film was used as the separator. The entire process of coin cell fabrication was conducted within an argon-filled glovebox with H_2O <0.1 ppm and O_2 <1 ppm. Cycling and capacity retention were measured using Neware battery test system between 3.0 and 4.3 V versus Li/Li^+ in different current densities at room temperature. Specific capacities and current densities were calculated on the basis of the weight of $LiCoO_2$.

For the purpose of comparison, CR2032 coin cells made of commercial $LiCoO_2$ powder (acquired from MTI Corp.) were also fabricated and tested. This powder will be termed as micro-$LiCoO_2$ hereafter because its particle sizes are in the micrometer range. The electrode made of micro-$LiCoO_2$ contained 80 wt % $LiCoO_2$, 10 wt % carbon black, and 10 wt % PVDF. Other conditions in fabricating CR2032, such as the active material loading per unit area, Li anode, $LiPF_6$ electrolyte, Celgard 2325 separator, etc., were identical to those in fabricating CR2032 coin cells with the nano-$LiCoO_2$ electrodes. Note that the electrode made of nano-$LiCoO_2$ contained more carbon black (15 wt %) than the counterpart made of micro-$LiCoO_2$ (10 wt %) because nano-$LiCoO_2$ has a much larger surface area per unit volume than that of micro-$LiCoO_2$ and thus requires more carbon black to ensure all or most nano-$LiCoO_2$ particles are connected to the conductive carbon black network.[13]

The particle size and morphology of nano- and micro-$LiCoO_2$ powders were examined using a JEOL JSM-5900LV (JEOL Ltd., Tokyo, Japan) scanning electron microscope with an accelerating voltage of 20 kV. The JEOL JEM-2100F (JEOL Ltd., Tokyo, Japan) transmission electron microscope in the Center for Nanoscale Materials at Argonne National Laboratory was also employed to determine the particle size and morphology of nano-$LiCoO_2$ powder. The XRD patterns were recorded using Bruker D2 Phaser with a Bragg−Brentano geometry in the 2θ range of 10−100° with Cu Kα radiation (1.54056 Å). To provide good measurement of the lattice parameters (a and c) of $LiCoO_2$ whose space group is $R\bar{3}m$, 5 wt % micrometer-sized Si powder was mixed uniformly with the $LiCoO_2$ powder before the XRD experiment to serve as an internal reference. Rietveld refinement using GSAS software[14] was used to determine the lattice parameters and phase composition of the XRD patterns from various samples, whereas the crystallite sizes of nano- and micro-$LiCoO_2$ before battery testing were estimated using the Scherrer formula.[15]

For postmortem analysis, the half-cells cycled with different conditions were opened using a crimping machine in an Ar-filled glovebox. The cycled cathode was then washed with dimethyl carbonate (DMC) three times, followed by heating in a vacuum oven for 6 h to remove residue organics. After drying, the cathode along with the Al-foil disk was completely sealed with large Kapton tapes and kept inside the glovebox until XAS and XRD experiments. X-ray absorption spectra were collected at the Materials Research Collaborative Access Team (MRCAT) Sector 10 bending magnet beam line at the Advanced Photon Source using a Si(111) water-cooled double crystal monochromator detuned to 50% for harmonic rejection.[16] Data was collected both in transmission and fluorescence using standard ionization chambers and continuous scanning of the energy. Data reduction and fitting was performed using the IFEFFIT-based Horae suite.[17,18] All data were fitted in *R*-space using Hanning window functions, a *k*-space range of 2−12 $Å^{-1}$ with dk = 4 $Å^{-1}$ and an *R*-space range of 1−3 Å with dR = 0.2 Å.

RESULTS AND DISCUSSION

Figure 1 shows XRD patterns of nano- and micro-$LiCoO_2$ powders before electrochemical testing. It is obvious that nano-$LiCoO_2$ has the same XRD pattern as that of micro-$LiCoO_2$. However, nano-$LiCoO_2$ peaks are much broader than micro-$LiCoO_2$ peaks, indicating nanosizes of the $LiCoO_2$ particles synthesized through the hydrothermal reaction. The average size of nano-$LiCoO_2$ perpendicular to a given crystallographic plane (hkl), D_{hkl}, was estimated using the Scherrer formula[15]

$$D_{hkl} = \frac{0.9\lambda}{\beta_{\text{real}} \cos\theta} \tag{1}$$

where β_{real} is the broadening of the diffraction line (hkl) measured at half-maximum intensity, λ is the wavelength of the X-ray radiation, and θ is the Bragg angle. Correction for instrumental broadening was taken into account with the aid of the following equation[19]

$$\beta_{\text{real}}^2 = \beta_{\text{nano}}^2 - \beta_{\text{micron}}^2 \tag{2}$$

where β_{nano} and β_{micron} are the half-maximum breadths from nano-$LiCoO_2$ and micro-$LiCoO_2$, respectively. The estimated dimensions of $LiCoO_2$ nanoplates are listed in Table 1 along with the measured lattice parameters. The as-synthesized

DOI: 10.1021/acs.jpcc.8b10099
J. Phys. Chem. C XXXX, XXX, XXX−XXX

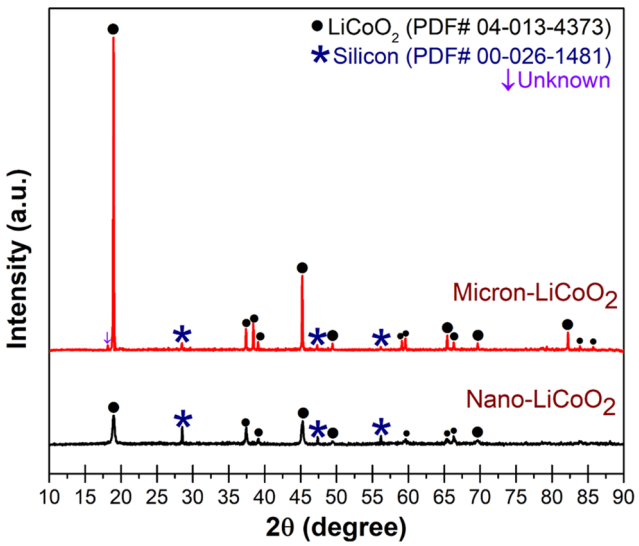

Figure 1. XRD patterns of nano-$LiCoO_2$ and micro-$LiCoO_2$ powders, as indicated. Micrometer-sized Si powder (5 wt %) was mixed with these powders uniformly as an internal reference.

Table 1. Powder Characteristics of Nano- and Micro-$LiCoO_2$

sample	a (Å)	c (Å)	c/a	D_{110} (nm)	D_{003} (nm)
nano-$LiCoO_2$	2.8162	14.0011	4.9716	38.7	23.9
micro-$LiCoO_2$	2.8200	14.0157	4.9701	NA	NA

$LiCoO_2$ nanoplates are estimated to have an average width of ~39 nm and an average height of ~24 nm. Note that the measured lattice parameters, a and c, are similar to those reported in ref 4. Furthermore, the c/a ratio for both nano-$LiCoO_2$ and micro-$LiCoO_2$ is close to 5.00, indicating that the as-synthesized nano-$LiCoO_2$ has the layered structure with space group of $R\bar{3}m$ rather than a spinel-type structure (cubic, $Fd\bar{3}m$).[4,20]

Figure 2a,b shows transmission electron microscopy (TEM) and scanning electron microscopy (SEM) images of nano- and micro-$LiCoO_2$ particles, respectively. It can be seen that micro-$LiCoO_2$ has very large particle sizes ranging from 3 to 15 μm and most of its particles have an equiaxed shape with flat facets in many cases. In contrast, nano-$LiCoO_2$ takes on a platelet morphology with a clear hexagonal, trapezoidal, or rhombus shape, reflecting the hexagonal crystal structure of $LiCoO_2$. The platelet width ranges from ~20 to 100 nm, confirming the estimation of the average width of ~39 nm from the XRD analysis. Although the height of the platelet cannot be judged from the TEM image of Figure 2a, it is reasonable to infer that the average height of the platelets is smaller than the average width of the platelets because most particles are lying with their basal planes in contact with the TEM carbon grid. Additional TEM images are provided in the Supporting Information where one or two nanoplates are standing up (Figure S1) and the thickness of the platelets determined from these images is ~23 nm, a number very close to the XRD analysis of ~24 nm. Thus, XRD analysis has provided good estimations for both the average width and height of the nano-$LiCoO_2$ platelets.

Galvanostatic charge/discharge curves of nano- and micro-$LiCoO_2$ half-cells are shown in Figure 3. These curves display three salient trends. First, at the charge/discharge rate of 1C (1C = 145 mA g^{-1}), nano-$LiCoO_2$ and micro-$LiCoO_2$ exhibit similar specific capacity (~130 mA h g^{-1} for the first discharge) and the length of the voltage plateau at ~3.85 V during discharge is similar for both nano- and micro-$LiCoO_2$, indicating that Li-ion intercalation and deintercalation can be accomplished for most of nano- and micro-$LiCoO_2$ particles in the electrodes at 1C (~90% utilization of 145 mA h g^{-1} for delithiation from $LiCoO_2$ to $Li_{0.47}CoO_2$ with the upper cutoff voltage at 4.3 V vs Li^+/Li). Interestingly, these phenomena also hold for 3C experiments but not 10C experiments. Second, as the charge/discharge rate increases from 1C to 3C and finally to 10C, the length of the voltage plateau of nano-$LiCoO_2$ keeps becoming shorter. The shorter voltage plateau may be induced by slow intercalation of Li ions at the electrode/electrolyte interface or slow diffusion of Li ions inside $LiCoO_2$ particles leading to incomplete utilization of the entire $LiCoO_2$ particles (to be discussed further later). Third, at the charge/discharge rate of 10C, nano-$LiCoO_2$ electrodes still display a discharge voltage plateau whereas micro-$LiCoO_2$ electrodes display a very short plateau with a slope-type profile. Note that many pseudocapacitors with intercalation of charge carriers on the electrode surface exhibit no voltage plateau behavior with a constant dQ/dV value for their discharge curves.[21−23] Thus, it may be concluded that at the 10C rate, the behavior of micro-$LiCoO_2$ is approaching that of a pseudocapacitor. However, the behavior of micro-$LiCoO_2$ is caused by slow intercalation of Li ions at the electrode/electrolyte interface, as will be discussed below. The three salient trends discussed above can

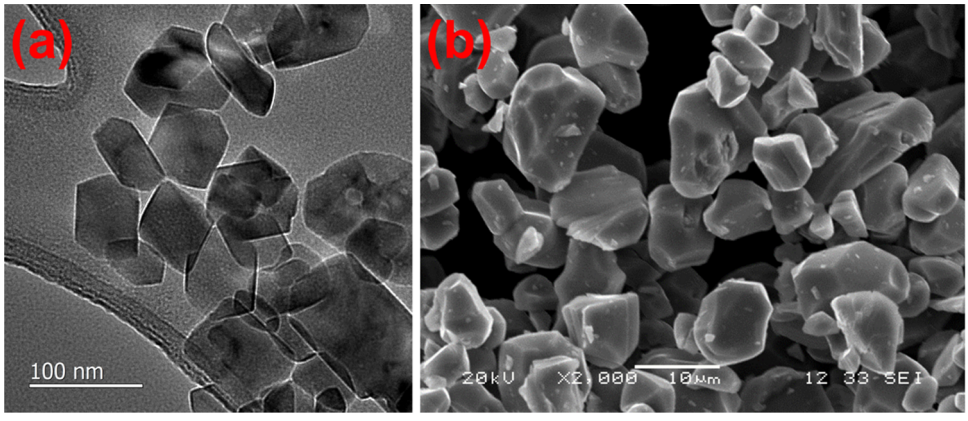

Figure 2. (a) TEM image of nano-$LiCoO_2$ and (b) SEM image of micro-$LiCoO_2$.

DOI: 10.1021/acs.jpcc.8b10099
J. Phys. Chem. C XXXX, XXX, XXX−XXX

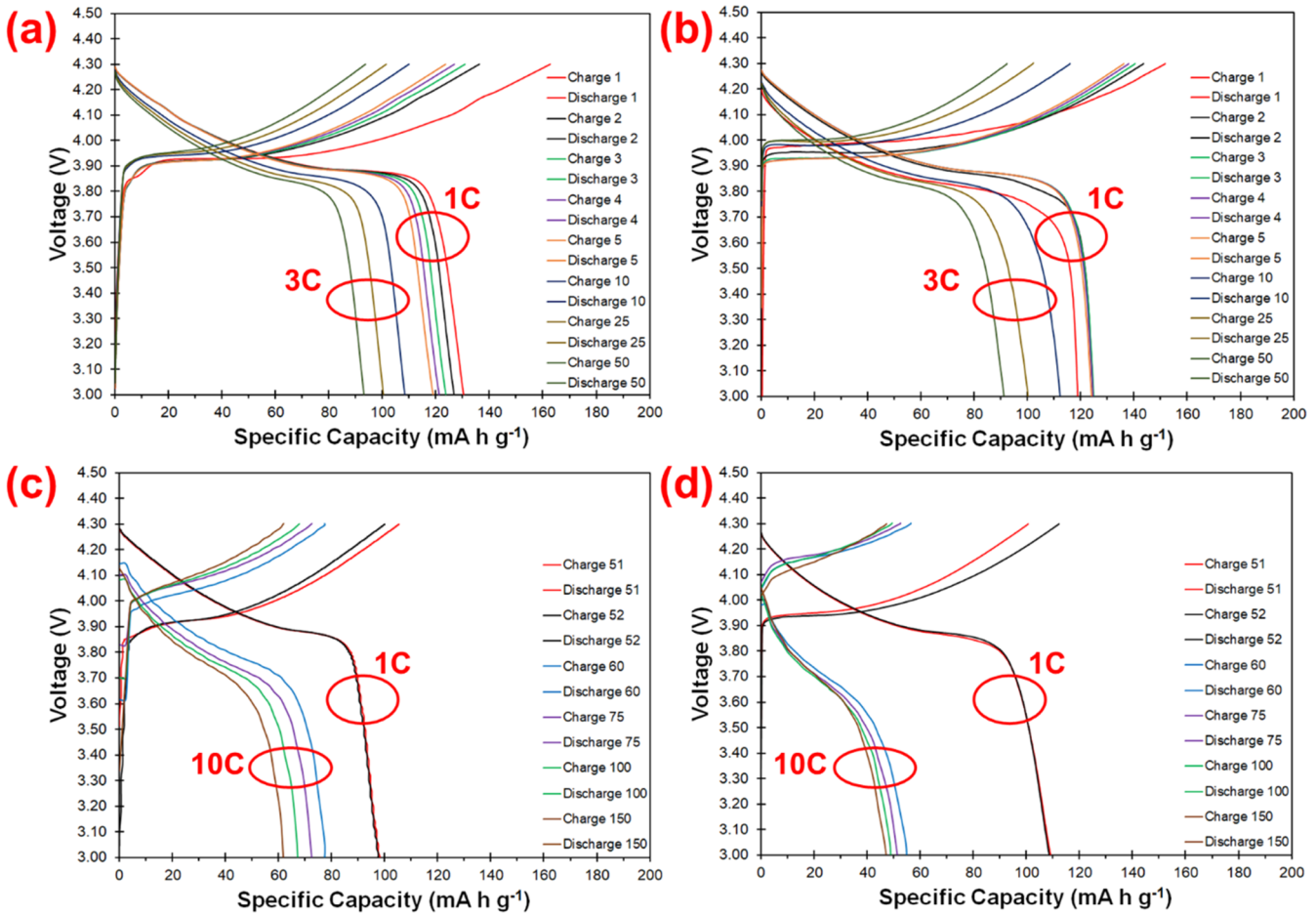

Figure 3. Charge/discharge curves: Both (a) nano-$LiCoO_2$ and (b) micro-$LiCoO_2$ were charged/discharged at 1C for 5 cycles and then 3C for 45 cycles; both (c) nano-$LiCoO_2$ and (d) micro-$LiCoO_2$ were charged/discharged at 10C for 500 cycles after 1C for 5 cycles, 3C for 45 cycles, and then 1C for 2 cycles. For the ease of observation, only selected charge/discharge curves are plotted.

be rationalized by analyzing the diffusion kinetics within $LiCoO_2$ particles, as described below.

First, the shorter voltage plateau is caused by slow Li-ion intercalation at the nano-$LiCoO_2$ surface rather than slow Li-ion diffusion inside $LiCoO_2$ nanoparticles. Assuming that diffusion constants, D_{Li}, of Li ions in micro- and nano-$LiCoO_2$ particles are the same, $D_{Li} = \sim 10^{-9}$ cm^2 s^{-1} reported in ref 24 can be used to estimate the diffusion time for a Li ion to diffuse from the surface to the center of a nano-$LiCoO_2$ particle (with an average diffusion distance of ~39 nm). This estimation reveals that it only takes $\sim 2.5 \times 10^{-3}$ s for a Li ion to diffuse from the surface to the center. Since the discharge time for 10C experiments (Figure 3c) is about 3 min, which is 5 orders of magnitude larger than the required diffusion time ($\sim 10^{-3}$ s) inside a nanoparticle, it can be concluded that the Li-ion intercalation rate at the electrode/electrolyte interface is very slow and thus is the rate-limiting step for Li-ion transport during discharge. As the discharge time increases from ~3 min for 10C experiments to ~12 min for 3C experiments and then to ~54 min for 1C experiments, more and more Li ions can be intercalated into Li_xCoO_2 ($x < 1$) particles and thus the voltage plateau becomes longer and longer. As a result, 1C experiments of nano-$LiCoO_2$ have the longest voltage plateau and the largest specific capacity among three charge/discharge rates. It should be noted that the length of the plateau is the manifestation of the collective behavior of all nano-$LiCoO_2$ particles even though individual particles are likely to contribute differently to the length of the plateau because of the heterogeneous nature of the electrode structure. A similar analysis can be applied to the delithiation process in charging of nano-$LiCoO_2$; i.e., deintercalation at the electrode/electrolyte interface is also very slow because it takes about 3 min to achieve the full charge at 10C, whereas the required Li diffusion time inside a nanoparticle is only $\sim 10^{-3}$ s. Therefore, it can be concluded that Li-ion intercalation and deintercalation at the electrode/electrolyte interface are the rate-limiting steps for discharge and charge of nano-$LiCoO_2$, respectively.

Second, by applying the same diffusion kinetic analysis to micro-$LiCoO_2$, it is found that it will take less than 1 min for a Li ion to diffuse from the surface to the center of a $LiCoO_2$ particle with a diameter of 10 μm. Note that a 1 min diffusion time is close to the charge/discharge time of 3 min at 10C experiments and thus it is difficult to identify the rate-limiting step for 10C experiments. However, 3C and 1C experiments take ~12 and ~54 min to complete, indicating that diffusion from the surface to the center of micro-$LiCoO_2$ particles can be easily accomplished (<1 min) and cannot be the rate-limiting step for lithiation and delithiation in discharge and charge of micro-$LiCoO_2$, respectively. Thus, the gradual decrease in the length of the voltage plateau and the specific capacity of micro-$LiCoO_2$ as the discharge rate increases from 1C to 3C and then to 10C can then be attributed to the

DOI: 10.1021/acs.jpcc.8b10099
J. Phys. Chem. C XXXX, XXX, XXX−XXX

gradually decreased time available for Li-ion intercalation at the electrode/electrolyte interface. Furthermore, as the Li-ion intercalation at the electrode/electrolyte interface is so slow that Li ions can only be lithiated to the particle surface region at 10C experiments, leading to the slope-type voltage profile. Thus, it can be concluded that the rate-limiting step for lithiation and delithiation of micro-$LiCoO_2$ is also Li-ion intercalation and deintercalation at the electrode/electrolyte interface. However, nano-$LiCoO_2$ particles have larger surface area per unit volume than that of micro-$LiCoO_2$ and thus can allow more Li^+ ions to intercalate and deintercalate at the electrode/electrolyte interface for a given discharge or charge voltage. As a result, nano-$LiCoO_2$ exhibits a longer voltage plateau and larger specific capacity than that of micro-$LiCoO_2$ when charge/discharge rates are high.

The precise mechanism for slow Li-ion intercalation and deintercalation at the electrode/electrolyte interface for both nano- and micro-$LiCoO_2$ is not known at this stage, but one of the possible mechanisms is the presence of a surface deterioration region (to be discussed later), which either has a very high resistance for Li-ion diffusion or requires high activation energies for Li ion to insert into and leave the surface of $LiCoO_2$. Regardless of the precise mechanism(s), the present study reveals unambiguously that to achieve the high-rate capability of $LiCoO_2$, not only do $LiCoO_2$ particle sizes need to be reduced to nanoscales but also the Li-ion intercalation and deintercalation rates at the electrode/electrolyte interface need to be enhanced.

The specific capacities of nano-$LiCoO_2$ and micro-$LiCoO_2$ as a function of charge/discharge cycle numbers are shown in Figure 4. As shown, nano- and micro-$LiCoO_2$ have similar specific capacities at 1C and 3C rates. However, micro-$LiCoO_2$ exhibits a sharper capacity drop than nano-$LiCoO_2$ when the charge/discharge rates are changed from 1C to 10C at the 53rd cycle, indicating that nano-$LiCoO_2$ is more suitable for high-rate applications because nano-$LiCoO_2$ has larger electrode/electrolyte interface area than that of micro-$LiCoO_2$ and this allows more Li^+ ions to deintercalate and intercalate at the electrode/electrolyte interface during charge and discharge, respectively. However, both nano- and micro-$LiCoO_2$ exhibit capacity decay as the cycle number increases. Although nano- and micro-$LiCoO_2$ have similar capacity decay rates, i.e., losing 53% specific capacity for nano-$LiCoO_2$ versus losing 49% specific capacity for micro-$LiCoO_2$ over 500 cycles at 10C, their capacity decay mechanisms are different. As will be shown later, the surface region of $LiCoO_2$ degrades gradually to become a CoO-dominated cobalt oxide layer, which leads to a loss of the charge storage capacity for nano-$LiCoO_2$ because the thickness of this CoO-dominated layer is similar to the size of nano-$LiCoO_2$ particles. Although such a CoO-dominated layer is also present at micro-$LiCoO_2$, this layer only accounts for less than 0.3% of the entire amount of micro-$LiCoO_2$ particles. Thus, the formation of this CoO-dominated surface layer causes very little change in the charge storage capacity of micro-$LiCoO_2$. However, the presence of this CoO-dominated surface layer and its growth have slowed down Li-ion intercalation and deintercalation at the electrode/electrolyte interface and thus resulted in its gradual capacity decay as the cycle number increases.

It is noted that the coulombic efficiencies of both nano- and micro-$LiCoO_2$ (defined as the discharge capacity divided by the charge capacity) are lower than 100% initially (Figure 4), owing to the formation of solid electrolyte interphase layer

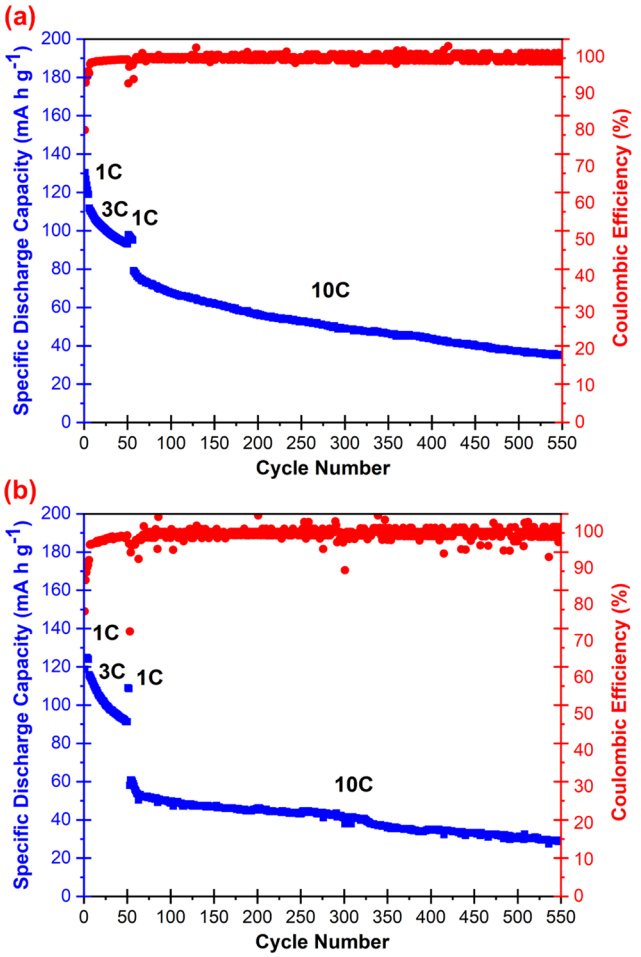

Figure 4. Specific capacity and coulombic efficiency vs cycle number for (a) nano-$LiCoO_2$ and (b) micro-$LiCoO_2$ with 1C for 5 cycles, 3C for 45 cycles, 1C for 2 cycles, and finally 10C for 500 cycles.

formation at the Li anode and the possible formation of a protection layer at the cathode side. However, nano-$LiCoO_2$ quickly exhibits nearly 100% coulombic efficiency after five cycles at 1C (Figure 4a), indicating the ability to attain stable charge/discharge cycling conditions quickly. In contrast, micro-$LiCoO_2$ displays a coulombic efficiency of lower than 100% for 5 cycles at 1C and then 45 cycles at 3C (Figure 4b), indicating that it requires more cycles than nano-$LiCoO_2$ to establish stable charge/discharge conditions, possibly due to different rates for Li-ion intercalation and deintercalation at the electrode/electrolyte interface at 3C for micro-$LiCoO_2$.

To identify the capacity decay mechanism(s), the cycled cathodes were analyzed using XRD and XAS. Figure 5 depicts the typical XRD patterns of nano- and micro-$LiCoO_2$ cathodes after some charge/discharge cycles. In these XRD patterns, Al peaks from the Al-foil current collector and the peaks from Kapton tapes are used to seal the sample and prevent the reaction of the cathode with air during XRD data collection. Although the XRD patterns of a Kapton tape and the Al foil with a Kapton tape can be found in the Supporting Information (Figures S2 and S3), these peaks are also marked in Figure 5 to facilitate the observation of cycled $LiCoO_2$ peaks. The Rietveld method has been applied to analyze these XRD patterns, and the major parameters obtained from these analyses are summarized in Table 2. Note that all samples in Table 2 are in the fully lithiated condition (i.e., after the

DOI: 10.1021/acs.jpcc.8b10099
J. Phys. Chem. C XXXX, XXX, XXX−XXX

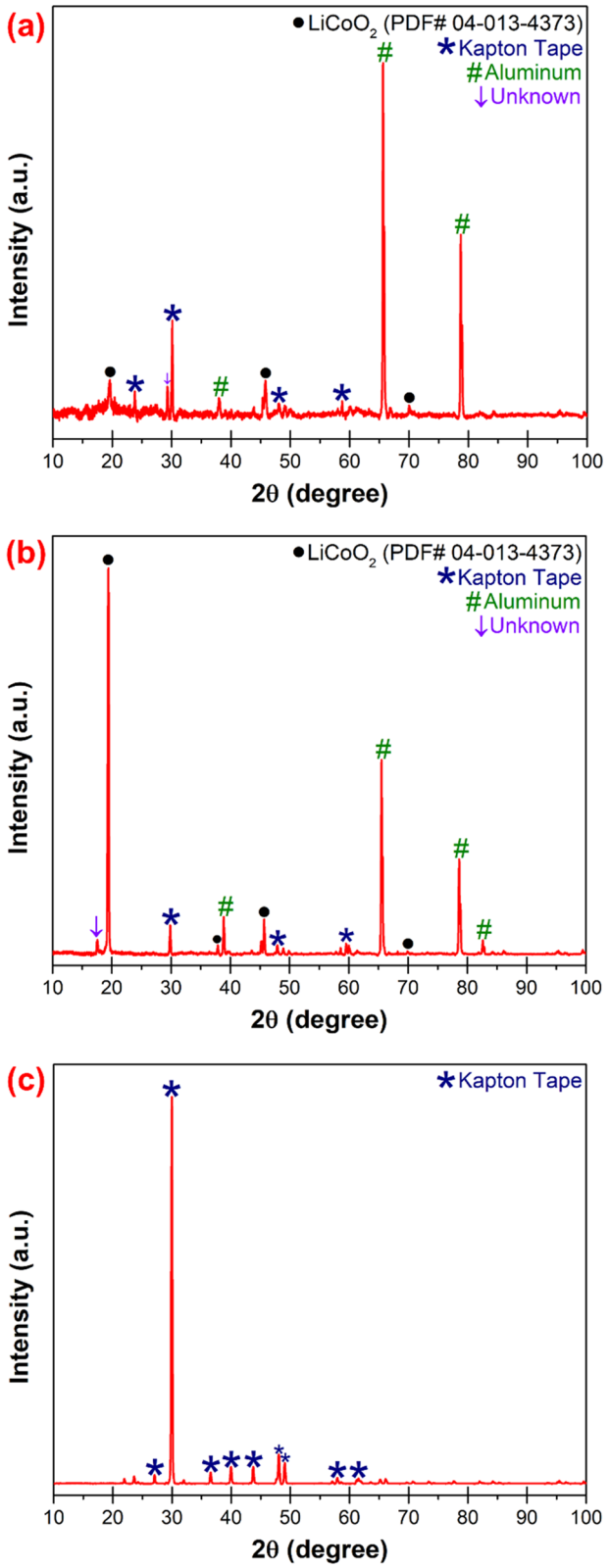

Figure 5. XRD patterns of the electrodes after charge/discharge cycling: (a) nano-$LiCoO_2$ electrode after 5 cycles at 1C and then 45 cycles at 3C, at fully lithiated condition, (b) micro-$LiCoO_2$ electrode after 5 cycles at 1C and then 45 cycles at 3C, at fully lithiated condition, and (c) the nano-$LiCoO_2$ cathode after 5 cycles at 1C and then 500 cycles at 10C, at fully lithiated condition. Note that the electrodes with Al foils are sealed by Kapton tapes and thus both Kapton and Al peaks are present in (a) and (b). However, the electrode in (c) has delaminated from the Al foil and thus Al peaks are absent. Further, no crystalline peaks of nano-$LiCoO_2$ are present in (c), indicating that nano-$LiCoO_2$ has become amorphous after 500 cycles at 10C.

desired cycles and finally being discharged to 3.0 V). Further, the phase composition of the electrode reported in the table is the relative concentration of crystalline compounds without the inclusion of amorphous phase(s). A comparison between Tables 1 and 2 reveals two salient trends. First, the lattice parameter c of both nano- and micro-$LiCoO_2$ has exhibited a discernible increase by 0.3−0.7% after cycling whereas the lattice parameter a has displayed little change (i.e., either increase by 0.1% or decrease by 0.1%). As a result, the c/a ratio has increased from 4.9716 for nano-$LiCoO_2$ to ∼5.0020 and from 4.9701 for micro-$LiCoO_2$ to 4.9924. The increased c/a ratio indicates the formation of Li-deficient $LiCoO_2$ for both nano- and microparticles after cycling. An earlier study[25] using density functional theory calculations has revealed that the lattice parameter c increases as a part of Li is removed from $LiCoO_2$. Such an increase in c is due to the weakened coulombic interaction between positively charged Li layers and negatively charged CoO_6 layers when part of the Li is removed from the lattice.[25] The formation of Li-deficient $LiCoO_2$ after cycling at the full lithiation condition shows that charge/discharge cycles have resulted in a loss of Li intercalation capability for both nano- and micro-$LiCoO_2$ when compared to that of their counterparts at the as-synthesized conditions.

The second important trend obtained by comparing Tables 1 and 2 is that after a large number of cycles (such as 10C for 500 cycles), crystalline nano-$LiCoO_2$ has become amorphous. Thus, by combining the XRD results of the electrodes with short cycles (such as nano-1, nano-2, and micro-1) and with long cycles (i.e., nano-3), one can conclude that charge/discharge cycles have led to gradual structural damage to $LiCoO_2$ crystals and eventually the structural damage is so large after a large number of cycles at fast charge/discharge rates that crystalline $LiCoO_2$ has become amorphous. However, more detailed structural analysis cannot be performed for the XRD patterns of cycled electrodes because $LiCoO_2$ peaks from these cycled electrodes are quite weak compared to the background. Consequently, the XRD data has unambiguously indicated the structural damage to cycled $LiCoO_2$ crystals but the specific damage mechanism(s) cannot be deduced from this analysis.

To gain additional insights into the degradation mechanisms, XAS analysis has been conducted. The X-ray absorption near edge structure (XANES) spectra of selected samples and standards are shown in Figure 6. The near-edge spectra of the micro-$LiCoO_2$ and the nano-$LiCoO_2$ samples are virtually identical and similar to those of nano-1, nano-2, and micro-1 samples, which are not shown. The edge of nano-3 sample (with 10C for 500 cycles) is shifted to lower energies and appears intermediate between the CoO and Co_3O_4 standards. The derivatives of the XANES spectra, shown in Figure S4 (Supporting Information), clearly indicate that nano-3 sample exhibits peak characteristics of Co_3O_4 and a shoulder at the peak position of CoO. Figure 7 presents the Fourier transform of the extended X-ray absorption fine structure (EXAFS) spectra for all samples, showing the similarity for all samples except nano-3. A comparison of the nano-3 Fourier transform

DOI: 10.1021/acs.jpcc.8b10099
J. Phys. Chem. C XXXX, XXX, XXX−XXX

Table 2. Powder Characteristics of Nano- and Micro-$LiCoO_2$ after Charge/Discharge Cycles[a]

sample	nano-1	nano-2	nano-3[b]	micro-1
cycling condition	1C for 5 cycles and then 3C for 45 cycles, at the fully lithiated condition	0.2C for 20 cycles, at the fully lithiated condition	1C for 5 cycles and then 10C for 500 cycles, at the fully lithiated condition	1C for 5 cycles and then 3C for 50 cycles, at the fully lithiated condition
phase composition of the electrode (wt %)	12.2% $CaCO_3$	21.2% $CaCO_3$	100% $CaCO_3$ amorphous $LiCoO_2$	6.8% $CaCO_3$
	19.0% $LiCoO_2$	13.0% $LiCoO_2$		15.9% $LiCoO_2$
	68.7% Al	65.7% Al		77.2% Al
a of $LiCoO_2$ (Å)	2.8195	2.8143	amorphous	2.8169
c of $LiCoO_2$ (Å)	14.1056	14.0742	amorphous	14.0630
c/*a* ratio	5.0029	5.0009		4.9924

[a]$CaCO_3$ is from Kapton tape, whereas Al is from the Al current collector. [b]The electrode is delaminated from the Al current collector during sample preparation after cycling.

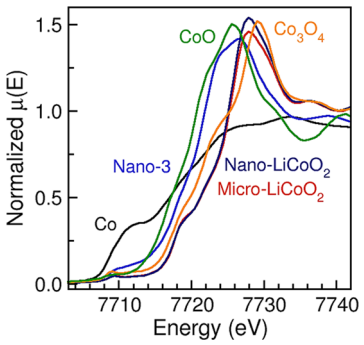

Figure 6. XANES spectra of pristine nano-$LiCoO_2$, pristine micro-$LiCoO_2$, and cycled nano-3 electrode along with selected standards. Other cycled electrode materials appear identical to the pristine materials. The spectra are color coded and matched with marks.

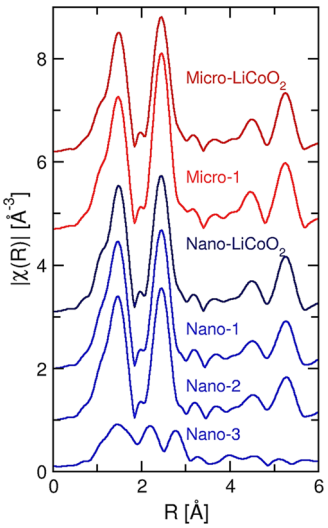

Figure 7. EXAFS Fourier transforms of pristine materials and cycled electrodes.

with the standards is shown in Figure S5 (Supporting Information). The $LiCoO_2$ peak at ~1.4 Å corresponding to Co−O distances is less intense and broader in nano-3 sample, and the peak at ~2.4 Å corresponding to Co−Co distances is split into two in nano-3 sample. In addition, nano-3 sample does not show the intense peaks at distances larger than 4 Å seen in all other samples. These long-distance peaks are typical of a well-ordered structure and imply that nano-3 has a severely damaged structure with only a short-range order, consistent with the conclusion of the presence of the amorphous phase in nano-3 derived from the XRD analysis. The EXAFS for all samples except for nano-3 were modeled using a near-neighbor Co−O1 path, a Co−Co path, and a long Co−O2 path which has significant overlap with the Co−Co path and whose coordination was held fixed at 6. For nano-3, the Co−Co path was split into two and fitted separately with a common σ^2. All samples were modeled with an amplitude reduction factor of 0.68 extracted from the fit of the nano-$LiCoO_2$ sample. Table 3 presents a compilation of the fit results for the Co−O and Co−Co paths for each sample and Figures S6−S11 (Supporting Information) present the EXAFS data and fits.

All samples except nano-3 have a Co−O1 bond distance of ~1.913 Å, a σ^2 of ~0.002 Å^2, and a coordination number of ~6 within their estimated standard deviations. Nano-3 sample, however, shows a significantly longer Co−O1 distance of 2.036 Å with a coordination number ~6 and σ^2 of ~0.015 Å^2. The results for the Co−Co paths present similar trends with all samples except for nano-3 having nearly identical parameters (R ~ 2.823 Å, N ~ 6, σ^2 ~ 0.003). Nano-3 has two Co−Co paths (R = 2.480 and 3.159 Å), with a total coordination number of 3.5.

Two important trends can be summarized from the XAS data discussed above. First, when the charge/discharge cycle number is small (e.g., nano-1 and nano-2 samples), their local and electronic structures are nearly identical to those of the pristine nanoparticles, indicating that charge/discharge cycles

Table 3. Fit Results of EXAFS Analysis

sample	R_{Co-O1}	σ_{Co-O1}^2	N_{Co-O1}	R_{Co-Co}	σ_{Co-Co}^2	N_{Co-Co}	R_{Co-O2}	σ_{Co-O2}^2
nano-$LiCoO_2$	1.194(6)	0.002(1)	6.0	2.818(5)	0.003(1)	6.2±0.9	3.409(66)	0.015(10)
nano-1	1.911(6)	0.003(1)	6.6 ± 0.6	2.824(6)	0.003(1)	6.7 ± 1.0	3.374(59)	0.012(8)
nano-2	1.910(6)	0.003(1)	6.5 ± 0.6	2.825(6)	0.003(1)	6.4 ± 1.0	3.366(57)	0.012(8)
nano-3	2.036(31)	0.015(6)	5.8 ± 1.8	2.480(14)	0.002(2)	1.5 ± 0.6	3.535(164)	0.035(42)
				3.159(16)		2.0 ± 0.9		
micro-$LiCoO_2$	1.914(6)	0.002(1)	5.3 ± 0.4	2.820(5)	0.002(1)	5.9 ± 0.7	3.416(59)	0.015(10)
micro-1	1.915(7)	0.002(1)	6.5 ± 0.7	2.821(5)	0.003(1)	8.0 ± 1.1	3.401(52)	0.008(8)

DOI: 10.1021/acs.jpcc.8b10099
J. Phys. Chem. C XXXX, XXX, XXX−XXX

are largely reversible with very limited structural damage. Second, when the charge/discharge cycle number is large (e.g., nano-3 with 10C for 500 cycles), both the Co K edge shift to lower energy and the longer Co−O1 bond length indicate that Co is in a lower oxidation state rather than the expected Co^{3+} after full lithiation, as exhibited by other nanosamples (e.g., nano-1 and nano-2). It is well known that delithiation during charging of micro-$LiCoO_2$ leads to oxidation of Co^{3+} to become Co^{4+} and the Co K edge displays a shift to higher energy whereas lithiation during discharging results in the Co K edge peak returning to its original position as Co^{4+} is reduced back to Co^{3+}.[26−28] Nano-1 and nano-2 samples follow this normal trend exhibited by micro-$LiCoO_2$.[26−28] However, nano-3 with a large number of cycles at a high rate (10C) displays anomalous behavior.

There are two likely mechanisms leading to the anomalous behavior exhibited by nano-3. First, a recent study using total-reflection XAS[29] has unambiguously revealed that when micro-$LiCoO_2$ electrode is in contact with the carbonate electrolyte during soaking, surface Co^{3+} ions are reduced to Co^{2+} ions by the electrolyte with the formation of a $Li_xCo_{1-x}O$ ($x < 1$) layer of ∼3 nm and other reaction products of Li_2CO_3 and/or lithium alkyl carbonate. The $Li_xCo_{1-x}O$ ($x < 1$) compound, which contains Co^{2+} ions through the replacement of a Li^+ ion by a Co^{2+} ion and another Co^{2+} located at the regular Co^{3+} site, is oxidized to become Co_3O_4 or other oxides in the subsequent charging process but with insufficient reduction in the discharging process. It is proposed that such a surface deterioration mechanism can continue in the subsequent charge/discharge processes, thereby leading to capacity decay over charge/discharge cycles.[29]

Another mechanism that leads to the formation of Co^{2+} ions for nano-3 is the overcharging effect induced by high charge rates (10C). Although the upper cutoff voltage in charging is only 4.3 V (vs Li^+/Li) in this study, the real potential experienced by the nano-$LiCoO_2$ cathode is actually higher than 4.3 V (vs Li^+/Li) because the high surface impedance of $LiCoO_2$ would require high overpotential to operate at 10C, exposing the cathode to a higher effective potential. The higher potential experienced by the cathode of a half-cell (with Li metal as the counter electrode) than the upper cutoff voltage is a well-known phenomenon. For instance, even at the 1C rate, a $Li(Ni_{0.5}Mn_{0.3}Co_{0.2})O_2$ cathode has experienced a potential of 4.38 V (vs Li^+/Li) when the half-cell upper cutoff voltage is at 4.30 V.[30] In our case, the cathode potential will be much higher than 4.3 V because the 10C rate is used and the overpotential increases with increasing current. A high overpotential means overcharging of the $LiCoO_2$ cathode (i.e., beyond 50% charge with the cathode potential much higher than 4.3 V vs Li^+/Li). A recent study[31] using electron energy-loss spectroscopy has revealed that overcharging of micro-$LiCoO_2$ cathodes results in the formation of a thin cobalt oxide layer (changing gradually from the surface CoO to the sub-surface Co_3O_4) on the surface region of $LiCoO_2$ particles, which is followed by an oxygen-deficient layer with composition of $Li_xCoO_{2-\delta}$ ($0 < x \leq 0.05$, $0 < \delta \leq 0.67$) before reaching the center of stoichiometric $LiCoO_2$.[31] In fact, the formation of CoO-like phases and the loss of lattice oxygen are found to initiate at 40% charge (namely, at ∼4.1 V vs Li^+/Li) and the surface layer of CoO-like phases reaches ∼5 nm after the first charge of 60%.[31] Repeated charge/discharge cycling will cause the progression of Co^{3+}/Co^{2+} reduction with loss of lattice oxygen from the surface region to the center of particles.[31] Accordingly, Co^{3+}/Co^{2+} reduction is expected to be much more prominent for nano-$LiCoO_2$ than micro-$LiCoO_2$ because nanoparticles have much larger surface area per unit volume. As discussed before, the nano-$LiCoO_2$ in this study is composed of 20 nm thick nanoplates whereas the micro-$LiCoO_2$ has particle sizes ranging from ∼3 to 10 μm. Assuming that nanoplates and microparticles achieve CoO-like phases at the surface region at the same rate, when an entire $LiCoO_2$ nanoplate achieves CoO-like phases, a micro-$LiCoO_2$ particle only has a 10 nm surface layer of CoO-like phases, which only accounts for 0.3−0.1% of the entire micro-$LiCoO_2$ material. As a result, the XANES spectrum of micro-$LiCoO_2$ cannot reveal the presence of Co^{2+} species even though surface deterioration on achieving CoO-like phases occurs. The XANES spectra of nano-1 and nano-2 do not exhibit the presence of Co^{2+} species either because they have only been subjected to relatively low-rate (0.2C, 1C, and/or 3C) charge/discharge cycles with limited cycle numbers (<50 cycles), thereby limited formation of CoO-like phases at the surface and the absence of Co^{2+} species in their XANES spectra.

It should be mentioned that the two mechanisms for the formation of Co^{2+} ions discussed above are likely operating in all $LiCoO_2$ samples. The first mechanism of reducing the surface Co^{3+} ions to Co^{2+} by the electrolyte occurs predominantly during soaking, whereas the second mechanism of forming the CoO-like surface region due to overcharging operates in every charge cycle. Furthermore, the higher the charge rate, the faster is the progression of the CoO-like surface region into the center of $LiCoO_2$ particles. This is the reason why nano-1 and nano-2 samples do not exhibit Co^{2+} species in their XANES spectra because their charge rates (≤3C) are lower than that experienced by nano-3 (10C). This phenomenon also suggests that reducing the surface Co^{3+} ions to Co^{2+} by the electrolyte during soaking does not produce enough Co^{2+} ions that can be detected by the XAS experiment used in this study. As for micro-1 sample, it does not display Co^{2+} species in its XANES spectrum because the CoO-like surface region only accounts for ≤0.3% of its entire material. With these understandings, it can now be concluded that the capacity decay of nano-$LiCoO_2$ over charge/discharge cycles at 10C (Figure 4a) is due to the gradual loss in the charge storage capacity as the CoO-like surface region grows into the center of nano-$LiCoO_2$. In contrast, the capacity decay of micro-$LiCoO_2$ over cycles at 10C (Figure 4b) is related to the gradual growth of the CoO-like surface region that slows down Li-ion intercalation and deintercalation at the electrode/electrolyte interface. For practical applications, since the mechanism of reducing Co^{3+} ions to Co^{2+} starts at the surface, proper coatings have the potential to prevent the formation of Co^{2+} and thus minimize the capacity decay of nano-$LiCoO_2$ over charge/discharge cycles at high rates. Such a potential has been demonstrated with thin and uniform Al_2O_3 coatings deposited on submicron $LiCoO_2$ particles (200−700 nm in size) using atomic layer deposition (ALD), leading to stable cycle stability with no loss of the specific capacity for 200 cycles at 2.8C.[5] In addition to this prior study, our group is currently investigating a new wet-chemical coating method that has lower costs than ALD but still offers significant improvement in the charge/discharge cycle stability of nano-$LiCoO_2$.[32] The coating material, method, and conditions, as well as the electrochemical improvement of coated nano-$LiCoO_2$ over pristine nano-$LiCoO_2$ will be communicated in a future publication.[32]

DOI: 10.1021/acs.jpcc.8b10099
J. Phys. Chem. C XXXX, XXX, XXX−XXX

Before closing, it should be pointed out that although the nano-$LiCoO_2$ in this study is synthesized using the method established in ref 4, direct comparisons in the electrochemical performance between ref 4 and the present study cannot be made. This is due to the difference in the charge/discharge protocol. The experiments conducted in ref 4 entailed charging at 1C and then discharging at different rates, including 1C, 30C, 50C, and 100C, whereas the experiments in this study have the same fast charging and discharging rates (i.e., at 3C or 10C) and thus are more close to practical applications wherein fast charging is desired. Furthermore, only 20 cycles of charging at 1C and then discharging at 10C were performed in ref 4 whereas 500 cycles of fast charging/discharging at 10C are conducted in this study. In spite of the difference in the charge/discharge protocol, two observations can be made. First, the discharge capacity (130 mA h g^{-1}) of the first charge/discharge cycle of this study with both charging and discharging at 1C is similar to that reported in ref 4 (~125 mA h g^{-1}). Second, the specific capacity decay in 20 cycles of charging at 1C and then discharging at 10C reported in ref 4 is ~32%, which is larger than the specific capacity decay of ~20% in 5 charge/discharge cycles at 1C and then 15 charge/discharge cycles at 3C in this study. Clearly, in both cases, the fast decay in the specific capacity is not acceptable for any practical applications and therefore coating strategy should be pursued if nano-$LiCoO_2$ is to be utilized for high-power applications. As pointed out before, such a coating strategy with a novel wet-chemical method is currently under investigation in our group and the preliminary result indicates very promising results that will be communicated in a future publication.[32]

CONCLUSIONS

Detailed analysis of the charge/discharge behavior of nano-$LiCoO_2$ over 500 cycles at the 1C, 3C, and 10C rates has been performed for the first time. The postmortem analysis of the cycled nano-$LiCoO_2$ cathodes using a combination of XAS and XRD has also been conducted, for the first time, to develop the mechanistic understanding of the charge/discharge behavior of nano-$LiCoO_2$ over 500 cycles at high rates. The behavior of nano-$LiCoO_2$ has been compared with that of micro-$LiCoO_2$ to identify the potential advantages of nano-$LiCoO_2$ over micro-$LiCoO_2$ and the challenges faced by nano-$LiCoO_2$ for high-rate applications. The following conclusions can be drawn from this investigation.

(i) Galvanostatic charge/discharge cycles at 10C have resulted in gradual structural damage to crystalline nano-$LiCoO_2$, and eventually the structural damage is so large after 500 charge/discharge cycles that crystalline nano-$LiCoO_2$ has become amorphous.

(ii) XAS analysis shows that nano-$LiCoO_2$ after 500 charge/discharge cycles at 10C has a severely damaged structure with only a short-range order, consistent with the XRD analysis.

(iii) XAS analysis also reveals the presence of Co^{2+} species in nano-$LiCoO_2$ at the fully lithiated condition after 500 charge/discharge cycles at 10C. The longer Co−O bond length exhibited by nano-$LiCoO_2$ after 500 cycles also indicates that Co is in a lower oxidation state rather than the expected Co^{3+} after full lithiation.

(iv) The specific capacity decay displayed by nano-$LiCoO_2$ over charge/discharge cycles at the 10C rate is mainly due to the gradual loss of the charge storage capacity of nano-$LiCoO_2$, induced by the structural damage, formation of CoO-like phases in the surface region, and gradual progression of the CoO-like surface region into the center of nano-$LiCoO_2$ particles over charge/discharge cycles at 10C.

(v) The capacity decay of micro-$LiCoO_2$ over charge/discharge cycles at 10C is, however, related to the gradual growth of the CoO-like surface region that gradually slows down Li-ion intercalation and deintercalation at the electrode/electrolyte interface as the cycle number increases.

(vi) The voltage plateau at ~3.85 V during discharge becomes shorter for both nano- and micro-$LiCoO_2$ as the discharge rate increases from 1C to 3C and finally 10C. This phenomenon is caused by slow intercalation of Li ions at the electrode/electrolyte interface.

(vii) The rate-limiting steps for lithiation and delithiation of nano- and micro-$LiCoO_2$ are Li-ion intercalation and deintercalation at the electrode/electrolyte interface. Thus, to achieve the high-rate capability of $LiCoO_2$, not only $LiCoO_2$ particle sizes need to be reduced to nanoscales but also the Li-ion intercalation and deintercalation rates at the electrode/electrolyte interface need to be enhanced.

(viii) The slow Li-ion intercalation and deintercalation at the electrode/electrolyte interface is likely related to the structural damage and/or the formation of CoO-like phases in the surface region. Since the both degradations above start at the electrode/electrolyte interface, proper coatings have the potential to solve this problem as well as minimizing the capacity decay of nano-$LiCoO_2$ over long-term cycles at high rates.

ASSOCIATED CONTENT

Supporting Information

The Supporting Information is available free of charge on the ACS Publications website at DOI: 10.1021/acs.jpcc.8b10099.

Additional TEM images, XRD patterns, XANES spectra, and EXAFS data (PDF)

AUTHOR INFORMATION

Corresponding Author

*E-mail: lshaw2@iit.edu.

ORCID

Carlo Segre: 0000-0001-7664-1574

Leon Shaw: 0000-0002-2170-1573

Notes

The authors declare no competing financial interest.

ACKNOWLEDGMENTS

This study was conducted as an Interprofessional Project (IPRO) at Illinois Institute of Technology. The financial support to this IPRO project from Wanger Institute for Sustainable Energy Research (WISER) and Rowe Family Endowment Fund is greatly appreciated. The experiments performed in this IPRO project by undergraduate students, San Dinh, Yuxia Fang, Washeq Khan, Kevin Little, Ben Martin, Sam Montag, John Munoz, Ricky Nguyen, Bowen Sun, Yuan Wang, Yu Zhou, and graduate student, Mei Luo, are acknowledged.

DOI: 10.1021/acs.jpcc.8b10099
J. Phys. Chem. C XXXX, XXX, XXX−XXX

REFERENCES

(1) Tarascon, J. M.; Armand, M. Issues and Challenges Facing Rechargeable Lithium Batteries. *Nature* **2001**, *414*, 359−367.

(2) Gordon-Bloomfield, N. *How Fast Does a Tesla Supercharger Charge an Electric Tesla Model S?* https://transportevolved.com/2014/07/03/fast-tesla-supercharger-charge-electric-tesla-model-s-fast/ (accessed 25 June, 2017).

(3) Somerville, L.; Bareño, J.; Trask, S.; Jennings, P.; McGordon, A.; Lyness, C.; Bloom, I. The Effect of Charging Rate on the Graphite Electrode of Commercial Lithium-Ion Cells: A Post-Mortem Study. *J. Power Sources* **2016**, *335*, 189−196.

(4) Okubo, M.; Hosono, E.; Kim, J.; Enomoto, M.; Kojima, N.; Kudo, T.; Zhou, H.; Honma, I. Nanosize Effect on High-Rate Li-Ion Intercalation in $LiCoO_2$ Electrode. *J. Am. Chem. Soc.* **2007**, *129*, 7444−7452.

(5) Scott, I. D.; Jung, Y. S.; Cavanagh, A. S.; Yan, Y.; Dillon, A. C.; George, S. M.; Lee, S.-H. Ultrathin Coatings on Nano-$LiCoO_2$ for Li-Ion Vehicular Applications. *Nano Lett.* **2011**, *11*, 414−418.

(6) Peng, Z. S.; Wan, C. R.; Jiang, C. Y. Synthesis by Sol−Gel Process and Characterization of $LiCoO_2$ Cathode Materials. *J. Power Sources* **1998**, *72*, 215−220.

(7) Yoon, W.-S.; Kim, K.-B. Synthesis of $LiCoO_2$ Using Acrylic Acid and Its Electrochemical Properties for Li Secondary Batteries. *J. Power Sources* **1999**, *81*−*82*, 517−523.

(8) Li, Y.; Wan, C.; Wu, Y.; Jiang, C.; Zhu, Y. Synthesis and Characterization of Ultrafine $LiCoO_2$ Powders by a Spray-Drying Method. *J. Power Sources* **2000**, *85*, 294−298.

(9) Chen, H.; Qiu, X.; Zhu, W.; Hagenmuller, P. Synthesis and High Rate Properties of Nanoparticled Lithium Cobalt Oxides as the Cathode Material for Lithium-Ion Battery. *Electrochem. Commun.* **2002**, *4*, 488−491.

(10) Chen, H.; Grey, C. P. Molten Salt Synthesis and High Rate Performance of the "Desert-Rose" Form of $LiCoO_2$. *Adv. Mater.* **2008**, *20*, 2206−2210.

(11) Liang, H.; Qiu, X.; Chen, H.; He, Z.; Zhu, W.; Chen, L. Analysis of High Rate Performance of Nanoparticled Lithium Cobalt Oxides Prepared in Molten KNO_3 for Rechargeable Lithium-Ion Batteries. *Electrochem. Commun.* **2004**, *6*, 789−794.

(12) Jiao, F.; Shaju, K. M.; Bruce, P. G. Synthesis of Nanowire and Mesoporous Low-Temperature $LiCoO_2$ by a Post-Templating Reaction. *Angew. Chem., Int. Ed.* **2005**, *44*, 6550−6553.

(13) Wang, C.; Sawicki, M.; Emani, S.; Liu, C.; Shaw, L. L. $Na_3MnCO_3PO_4$ − a High Capacity, Multi-Electron Transfer Redox Cathode Material for Sodium Ion Batteries. *Electrochim. Acta* **2015**, *161*, 322−328.

(14) Larson, A. C.; Von Dreele, R. B. *General Structure Analysis System (GSAS)*; Los Alamos National Laboratory: New Mexico, 2004.

(15) Klug, H. P.; Alexander, L. E. *X-ray Diffraction Procedures: For Polycrystalline and Amorphous Materials*; Wiley, 1974.

(16) Kropf, A. J.; et al. The New MRCAT (Sector 10) Bending Magnet Beamline at the Advanced Photon Source. *AIP Conf. Proc.* **2010**, *1234*, 299−302.

(17) Newville, M. IFEFFIT: Interactive XAFS Analysis and FEFF Fitting. *J. Synchrotron Radiat.* **2001**, *8*, 322−324.

(18) Ravel, B.; Newville, M. Athena, Artemis, Hephaestus: Data Analysis for X-ray Absorption Spectroscopy Using IFEFFIT. *J. Synchrotron Radiat.* **2005**, *12*, 537−541.

(19) Shaw, L. L.; Yang, Z. G.; Ren, R. M. Synthesis of Nanostructured Si_3N_4/SiC Composite Powders through High Energy Reaction Milling. *Mater. Sci. Eng., A* **1998**, *244*, 113−126.

(20) Gummow, R. J.; Thackeray, M. M.; David, W. I. F.; Hull, S. Structure and Electrochemistry of Lithium Cobalt Oxide Synthesised at 400 °C. *Mater. Res. Bull.* **1992**, *27*, 327−337.

(21) Yang, L.; Cheng, S.; Ji, X.; Jiang, Y.; Zhou, J.; Liu, M. Investigations into the Origin of Pseudocapacitive Behavior of Mn_3O_4 Electrodes Using in Operando Raman Spectroscopy. *J. Mater. Chem. A* **2015**, *3*, 7338−7344.

(22) Ji, X.; Cheng, S.; Yang, L.; Jiang, Y.; Jiang, Z.-j.; Yang, C.; Zhang, H.; Liu, M. Phase Transition−Induced Electrochemical Performance Enhancement of Hierarchical $CoCO_3$/CoO Nanostructure for Pseudocapacitor Electrode. *Nano Energy* **2015**, *11*, 736−745.

(23) Brousse, T.; Bélanger, D.; Long, J. W. To Be or Not to Be Pseudocapacitive? *J. Electrochem. Soc.* **2015**, *162*, A5185−A5189.

(24) Park, M.; Zhang, X.; Chung, M.; Less, G. B.; Sastry, A. M. A Review of Conduction Phenomena in Li-Ion Batteries. *J. Power Sources* **2010**, *195*, 7904−7929.

(25) Xiong, F.; Yan, H.; Chen, Y.; Xu, B.; Le, J.; Ouyang, C. The Atomic and Electronic Structure Changes Upon Delithiation of $LiCoO_2$: From First Principles Calculations. *Int. J. Electrochem. Sci.* **2012**, *7*, 9390−9400.

(26) Yoon, W.-S.; Kim, K.-B.; Kim, M.-G.; Lee, M.-K.; Shin, H.-J.; Lee, J.-M.; Lee, J.-S.; Yo, C.-H. Oxygen Contribution on Li-Ion Intercalation−Deintercalation in $LiCoO_2$ Investigated by O K-Edge and Co L-Edge X-Ray Absorption Spectroscopy. *J. Phys. Chem. B* **2002**, *106*, 2526−2532.

(27) Balasubramanian, M.; Sun, X.; Yang, X. Q.; McBreen, J. In Situ X-Ray Absorption Studies of a High-Rate $LiNi_{0.85}Co_{0.15}O_2$ Cathode Material. *J. Electrochem. Soc.* **2000**, *147*, 2903−2909.

(28) Patridge, C. J.; Love, C. T.; Swider-Lyons, K. E.; Twigg, M. E.; Ramaker, D. E. In-Situ X-Ray Absorption Spectroscopy Analysis of Capacity Fade in Nanoscale-$LiCoO_2$. *J. Solid State Chem.* **2013**, *203*, 134−144.

(29) Takamatsu, T.; Koyama, Y.; Orikasa, Y.; Mori, S.; Nakatsutsumi, T.; Hirano, T.; Tanida, H.; Arai, H.; Uchimoto, Y.; Ogumi, Z. First in Situ Observation of the $LiCoO_2$ Electrode/Electrolyte Interface by Total-Reflection X-Ray Absorption Spectroscopy. *Angew. Chem., Int. Ed.* **2012**, *51*, 11597−11601.

(30) Gilbert, J. A.; Shkrob, I. A.; Abraham, D. P. Transition Metal Dissolution, Ion Migration, Electrocatalytic Reduction and Capacity Loss in Lithium-Ion Full Cells. *J. Electrochem. Soc.* **2017**, *164*, A389−A399.

(31) Kikkawa, J.; Terada, S.; Gunji, A.; Nagai, T.; Kurashima, K.; Kimoto, K. Chemical States of Overcharged $LiCoO_2$ Particle Surfaces and Interiors Observed Using Electron Energy-Loss Spectroscopy. *J. Phys. Chem. C* **2015**, *119*, 15823−15830.

(32) Chen, C.; Yao, W.; He, Q.; Ashuri, M.; Liu, Y.; Shaw, L. L. Tunable $LiAlO_2$/Al2O_3 Coating through a Wet-Chemical Method to Improve Cycle Stability of Nano-$LiCoO_2$. *ACS Appl. Energy Mater.*, submitted for publication, **2019**.

DOI: 10.1021/acs.jpcc.8b10099
J. Phys. Chem. C XXXX, XXX, XXX−XXX